DETECTING PINHOLES IN COATINGS WITH HYPERSPECTRAL IMAGING

J. L. Garrett, T. A. Johansen, M. Orlandić *

Norwegian University of Science and Technology
Trondheim, Norway

M. A. Bashir

Jotun AS
Sandefjord, Norway

B. Raeissi

DNV GL AS
Høvik, Norway

ABSTRACT

Coatings are critical to maintaining the integrity of industrial and offshore equipment, but defects reduce their effectiveness. Pinholes, locations on a coated surface which remain uncoated, are one kind of defect. They difficult to detect because of their small size. Here we investigate the possibility of using Hyperspectral imaging to find pinholes. Seven painted steel panels are imaged with a short wave infrared hyperspectral camera. Two target detection algorithms are tested for finding pinholes using two spectral signatures: steel and an underlayer of epoxy paint. One pinhole that occupies multiple pixels is identified, and several possible subpixel pinholes are detected for each target signature. We expect that further improvements to the characterization of the target signal, a better understanding of false positives and noise and improvements to the validation process will allow the detection of subpixel pinholes.

***Index Terms*—** Pinholes, coatings, Target detection

1. INTRODUCTION

A common method to prevent corrosion of metals in industrial and commercial applications is to apply an anti-corrosive coating. However, such coatings often suffer defects or failures which limit their performance [1]. Pinholes, often called holidays, are defects that can appear during the application and curing of a coating. These holes, which may either be present on the surface of the topcoat or continue directly through two coats, expose the substrate to corrosive conditions and ultimately make the coating irrelevant. Sizes of pinholes can range from few nanometers to a few hundred micrometers [2].

*This work was supported by the Research Council of Norway by project grant number 282287 (ADRASSO) and by the Research Council of Norway, Equinor, DNV GL and Sintef through the Centers of Excellence funding scheme, Grant 223254 - Center for Autonomous Marine Operations and Systems (AMOS).

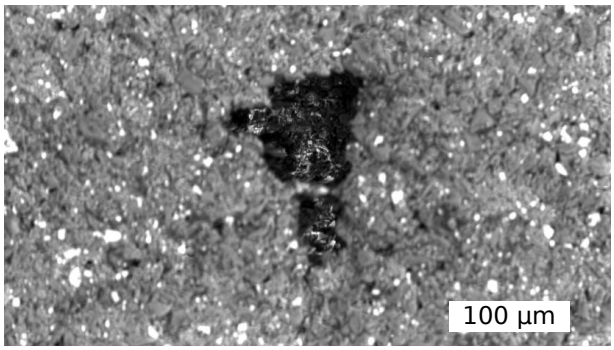

Fig. 1. Scanning electron microscope image of a pinhole.

Reasons for the formation of pinholes include high viscosity of the coating used, high evaporation rates of the solvents and thinners used, insufficient atomization and the entrapment of solvent or air in porous surface of the substrate.

Depending upon the size of pinholes, it may be difficult to detect them with a naked eye. Different high- and low-voltage holiday detectors are used to detect pinholes in commercial settings (Fig. 1). These high voltage pose a significant safety concern because they can operate up to 60,000 Volts which may seriously damage the operator and the coating [3, 4]. Deflectometry can be used to identify coating defects using a monochromatic or red-green-blue (RGB) camera, but it typically requires illumination and imaging sources to be physically separated [5, 6]. Moreover, at least one study has found that, relative to other defects, pinholes are a difficult defect to locate with deflectometry [7].

Hyperspectral imaging gives the possibility of looking for a particular target spectrum in a scene. Because a large portion of a material's optical response is recorded in the hyperspectral image, it is possible to look for sub-pixel targets [8]. In general, hyperspectral target detection algorithms look for targets by comparing the measured spectrum of each pixel to

both a background spectrum and a target spectrum. Target detection methods have previously been used to detect the presence of spectra that occupy as little as 5% of the area of the pixel [9]. Here we investigate the possibility of applying target detection to images captured by a hyperspectral camera to identify pinholes in industrial coatings.

This proceeding focuses on the short wave infrared (SWIR) portion of the electromagnetic spectrum, which spans wavelengths from 780 nm to 2500 nm. Light in this range of the spectrum can excite overtone and combination transitions of molecular vibrations, and electronic transitions of highly conjugated systems. Spectroscopy in this spectral range has been shown to be promising in polymer analysis because the absorption of SWIR radiation by the organic molecules is weak enabling greater path length flexibility and nondestructive sample analysis in both laboratory and process environments [10, 11]. Hyperspectral cameras can cover the same spectral range and provide compositional analysis results which are very similar to those provided by a laboratory scale near infrared spectroscope [12]. However, the coatings industry has not yet incorporated the use of such HSI cameras for the in-field detection of coating defects.

2. METHODS

Panels. Seven 15×7.5 cm steel panels are scanned for this experiment (Table 1). The panels each have different coatings. Two of the panels are coated with Safeguard Plus. The first of these two panels is coated at room temperature, as is typical, while the second is coated at 50 C. The paint is applied directly on the steel for the first panel, while on the second panel a layer of a Jotamastic 90 (JM90) intermediate underlayer, hereon referred to as primer, is also applied. Both of these commercial paints are based upon epoxy-amine system.

Table 1. Coated steel panels investigated

Coating	Preparation	Temperature
Hardtop XP	*Stirred*	*Room Temp*
Hardtop XP	Stirred	50 C
Hardtop XP	Shaken	Room Temp
Hardtop XP	Shaken	50 C
Hardtop XP	Shaken / Speedmixed	Room Temp
Safeguard Plus	Stirred	Room Temp
Safeguard Plus	Stirred	50 C

The other five panels are coated with a Hardtop XP White outerlayer and a JM90 underlayer. The paint was prepared in three different ways: by stirring (by hand), by shaking (mechanical), or by shaking-speedmixing (also mechanical). The panel with stirred paint, cured at room temperature is used for the in-depth analysis (denoted by italic text), and summary results are provided for the other panels.

The steel and primer target spectra are determined from the mean spectra of either a bare steel panel or a steel panel uniformly spray-coated with the JM90 primer (Fig. 2).

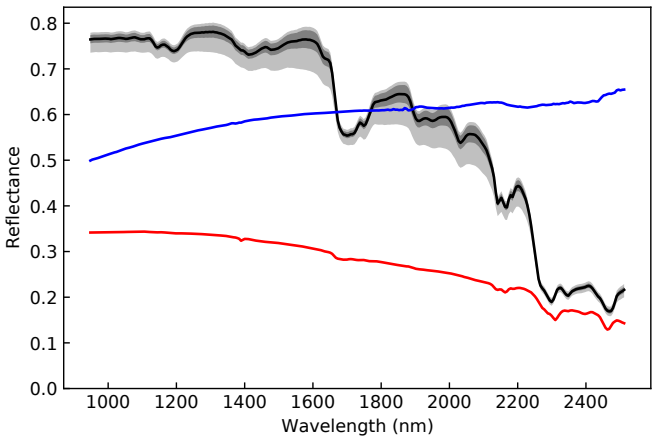

Fig. 2. Mean SWIR spectra of targets: steel (blue) and JM90 primer underlayer (red) together with mean background XP white spectra (black) with 1 or 2 standard deviations shaded (dark/light grey).

Hyperspectral imaging. Hyperspectral imaging is performed with the HySpex SWIR-384 (Norsk Elektro Optikk). The panels are scanned one-by-one over a low-reflectance background, with a known reference calibration in view as well. The panels are uniformly illuminated and the camera is held 300 mm from the panels. The procedure records an image of the panel that is about 600×300 pixels each consisting of 288 spectral bands. The resulting pixel spacing is about 0.22 mm. After an initial analysis of the results, the panels were scanned a second time with higher magnification at a pixel spacing of 0.052 mm. When imaging each panel, a reference gray tape is scanned as well.

Pre-processing. Reflectance data are used for the analysis. To prepare the reflectance datacubes, the acquired data are first converted to radiance with HySpex RAD software (Norsk Elektro Optikk AS). Next, the spectrum of the reference tape is used to convert the raw data into reflectance.

Target Detection. The matched filter (MF) is a common target detection algorithm, derived from a likelihood ratio test comparing two hypothesis: the presence of a target together with the background, and the absence of a target. It is defined as:

$$D_{\mathrm{MF}} = \frac{(\boldsymbol{x}-\boldsymbol{m})\boldsymbol{C}^{-1}(\boldsymbol{t}-\boldsymbol{m})}{(\boldsymbol{t}-\boldsymbol{m})\boldsymbol{C}^{-1}(\boldsymbol{t}-\boldsymbol{m})}, \tag{1}$$

where $\boldsymbol{x}$ is the pixel (a vector with reflectance at the sampled wavelengths) being analyzed, $\boldsymbol{m}$ is the mean of the background, $\boldsymbol{t}$ is the target being searched for, and $\boldsymbol{C}$ is the covariance matrix of the measured background. Note that the matched filter is normalized so that $D_{\mathrm{MF}} = 1$ when a pixel is completely filled with the target spectrum. With this normaliza-

tion, the output of the MF gives an estimate of the proportion of the pixel which is occupied by the target.

The adaptive cosine estimator (ACE) [13] is another hyperspectral target detection algorithm:

$$D_{\mathrm{ACE}} = \sqrt{\frac{(\boldsymbol{t}-\boldsymbol{m})\boldsymbol{C}^{-1}(\boldsymbol{t}-\boldsymbol{m})}{(\boldsymbol{x}-\boldsymbol{m})\boldsymbol{C}^{-1}(\boldsymbol{x}-\boldsymbol{m})}}D_{\mathrm{MF}}, \qquad (2)$$

It is based on separating a target signal from the background spectra in the image, and is derived from a generalized likelihood ratio test. ACE determines the cosine of the angle between the vector connecting the mean background spectrum to the target spectrum and the vector connecting the mean background spectrum to the spectrum of the pixel. Because, ACE is sensitive to target signatures even when they only occupy a small portion of the pixel area, it is also sensitive to noise. Therefore, MF is commonly combined with ACE in order to prevent noise from causing false detections.

After $\boldsymbol{C}$ and $\boldsymbol{m}$ are calculated, the sensitivity of the detectors is determined. The test spectrum is defined to be $\boldsymbol{x}(\lambda) = \lambda\boldsymbol{t} + (1-\lambda)\boldsymbol{m}$, where λ indicates the primer or steel proportion. Then the predicted response of a filter $\boldsymbol{D}$ to a pixel partially occupied by the target material is $\boldsymbol{D}(\boldsymbol{x}(\lambda))$, as shown in Fig. 3. In addition to the expected response of the detectors, shaded regions which show the effect of a $\pm 5\%$ change in the illumination intensity of the incident light are also plotted, in order to depict the effect of this common systematic error.

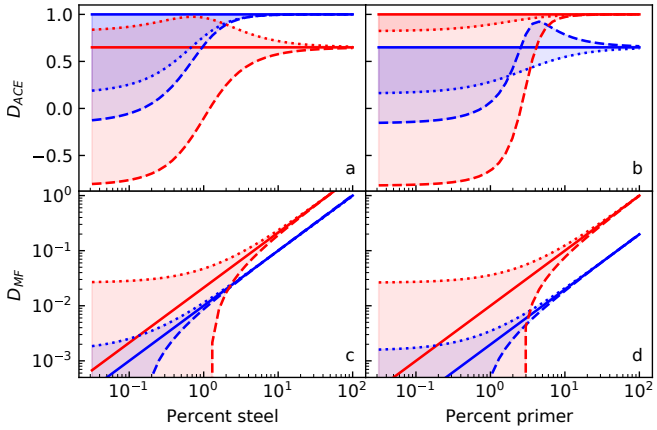

Fig. 3. Response of $\boldsymbol{D}_{\mathrm{ACE}}$ to mixed spectra to steel (blue) or primer (red) targets, with average (solid), 5% above-average (dotted) and below-average (dashed) illumination (a,b). Response of $\boldsymbol{D}_{\mathrm{MF}}$ the same mixed spectra (c,d).

3. RESULTS

Over the whole scanned panel, both detectors detect pixels with the primer target, but only the D_{ACE} detects pixels that could be steel (Fig. 4. Therefore, the subsequent analysis focuses on identifying locations that could be exposed primer. Note that the edges of the panel are fully coated with the primer but the top coat is either thin or not present. These edges are used to verify the operation of D_{ACE} and D_{MF} with the primer target signature. In the regions of exposed primer, the two detectors nearly follow their expected behavior (Fig. 5). The matched filter does exceed its expected value, which indicates that the in-scene spectrum of the primer differs some from the mean spectrum of the reference scene.

The magnified scan is used to inspect the location of one of the possible pinhole locations (Fig. 6). The D_{ACE} response peak in the magnified scan occupies several pixels, while the D_{MF} response is more localized. The spectra of the 4 pixels with the largest response are plotted against the background and target spectra (Fig. 7). Both the primer spectra from the reference panel, which is the target, and the in-scene primer spectra with or without a thin top coat are plotted for comparison. The in-scene spectra are calculated from the mean of exposed region (shown at the bottom of Fig. 4a). The in-scene primer spectra are much less reflective than the refe-

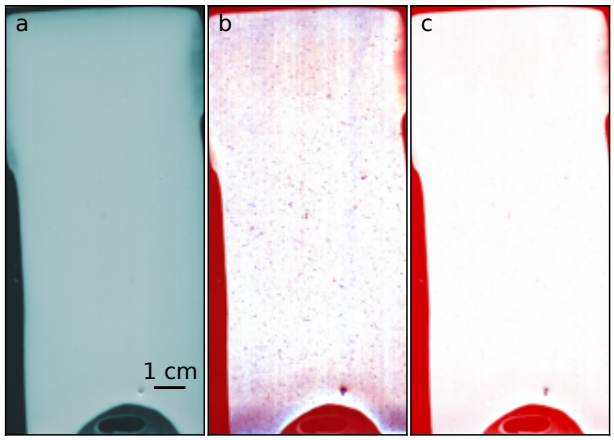

Fig. 4. A false color representation of the investigated panel (a). The response of the panel image to D_{ACE} with the steel (blue) or primer (red) target (b). The response of the panel image to D_{MF} (c).

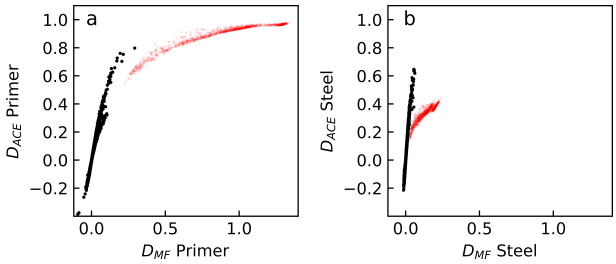

Fig. 5. (a) The response of the pixels on the painted region (black) and where primer is exposed (red) to the primer-target detectors. The response of the pixels to the steel-target (b).

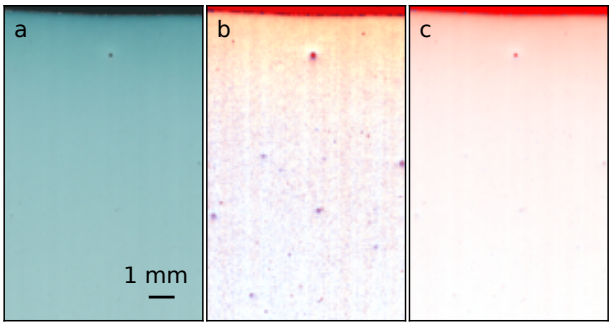

Fig. 6. An RGB representation of the small region of a panel with a pinhole at the center top (a). D_{ACE} applied to the location for the steel (blue) and primer (red) reference spectra (b). D_{MF} applied to the same location (c). Note that the red regions around the edges of the panel are exposed primer, and were excluded from the subsequent pinhole analysis.

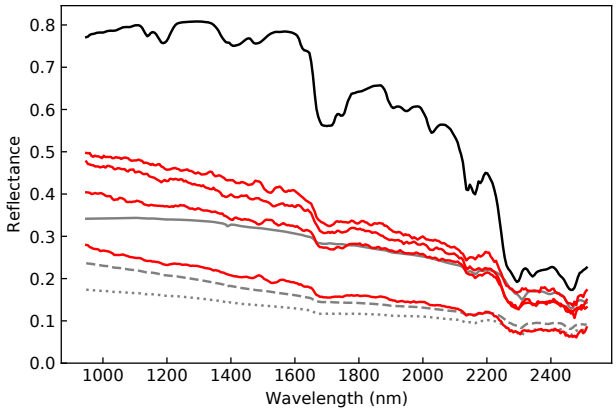

Fig. 7. The four spectra that achieved $D_{\mathrm{ACE}} > 0.9$ (red) for the primer signature at the location of the apparent pinhole in 6, compared to several mean spectra: the background (black), reference target (grey, solid), in-scene uncoated primer (grey, dotted), and in-scene primer under a thin top coat (grey-dashed).

rence spectra, and the in-scene spectra with a thin top coat is slightly more reflective than the one without. One pixel at the possible pinhole location shows a response that differs from the in-scene primer spectrum by about 5% at most, with most of the difference being below 1700 nm. The other three pixels show spectra that are more similar to the reference spectrum. This is consistent with a pinhole of a diameter of approximately 0.05-0.1 mm, which likely has a thin coating of top paint at the bottom.

One additional test of the ACE target detection methodology is the comparison of number of detected pinholes on several different panels. More pinholes are expected in in the coatings that were deposited at 50 C relative to room temperature and also more pinholes are expected on panels coated with paint that was stirred rather than shaken. Figure 8 shows the number of pixels marked as pinholes for various thresholds on the ACE and MF detector metrics. Most noticeable is the separation of the panels coated with Safeguard Plus from the panels coated with Hardtop XP white, which we hypothesize is caused by the greater similarity between the Safeguard Plus reflectance spectrum and the target spectra. Essentially, because both the coatings are epoxy-amine systems, their mean spectra are very similar.

4. CONCLUSION

When the ACE detector is used to search for pinholes on the coated steel panels, several candidate features are found. Where the primer is unambiguously exposed, both ACE and MF detect the primer, which shows that it does identify sufficiently large regions of the target material. At one particular location, a signal which strongly suggests a multi-pixel pinhole is identified. The spectra is most similar to the in-scene spectrum of primer with a thin top coat, which may indicate that there is a very thin layer of the top coat at the bottom of the pinhole. Further work will be necessary to confirm that there is a pinhole at that location, and to determine the size of the pinhole.

To develop this method into a reliable analysis tool, it will be necessary to determine how much of a pixel must be exposed primer in order to be detected. This will determine the resolution that a camera must have in order detect pinholes. There are some tactics which might improve the effective spatial resolution of a hyperspectral camera. For example, hyperspectral/multispectral fusion methods could be used to increase the effective spatial resolution of the camera.

Other target detectors may provide more accurate or faster performance. One impediment to fast target detection on low-power computers is the requirement of estimating $\boldsymbol{C^{-1}}$ and $\boldsymbol{m}$ [14]. It is possible to increase the speed of target detection by replacing $\boldsymbol{C^{-1}}$ with $\boldsymbol{R^{-1}}$, in which $\boldsymbol{R}$ is the correlation matrix, and eliminating $\boldsymbol{m}$ altogether from the detectors. When this is done to the matched filter, it becomes the constrained energy minimization (CEM) detector [15]. The corresponding variant of ACE is then called $\mathrm{ACE_R}$. Previous work showed that $\mathrm{ACE_R}$ can achieve comparable results when combined with dimensionality reduction [14].

These initial target detection tests show that HSI is a promising technique for detecting pinholes in coatings. When the exposed layer covers several pixels, target detection is able to detect it. These HSI techniques offer safety and scalability advantages relative to high-voltage contact measurements. Relative to RGB cameras, HSI is not limited to surfaces that exhibit specular reflection, and it is suitable to mounting the camera and illumination source on a single platform. Moreover, unlike the RGB-based techniques, when it finds a pinhole, it provides information about which underlayer is exposed.

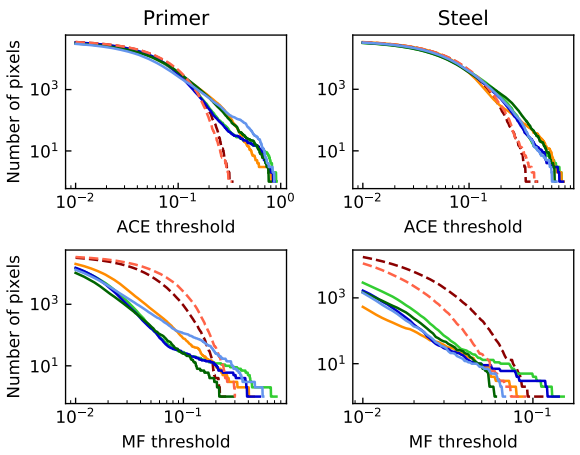

Fig. 8. The the number of pixels marked as pinholes using the ACE or MF detector, for both primer and steel, for several different panels. Seven panels are shown in total: the lighter lines of each color show paint applied at 50 C, while the darker line shows paint applied at room temperature. The red lines correspond to panels coated with Safegard Plus. The other colors correspond to how the paint was mixed: stirred (green), shaken (blue) shaken-speedmix (orange).

5. REFERENCES

[1] Krystel Pélissier and Dominique Thierry, "Powder and High-Solid Coatings as Anticorrosive Solutions for Marine and Offshore Applications? A Review," *Coatings*, vol. 10, no. 10, pp. 916, Sept. 2020.

[2] Edward D. Cohen and Ronald Grotovsky, "Digital image analysis of coating defects," *Progress in Organic Coatings*, vol. 22, no. 1-4, pp. 125–143, May 1993.

[3] NACE International, "High-voltage electrical inspection of pipeline coatings," Standard Recommended Practice RP0274-98, NACE International, Houston, TX, 2004, OCLC: 74811578.

[4] Thomas Belli, "Holidays and Pinholes: The Chink in the Armour," *Paint & coatings industry magazing*, Aug. 2016.

[5] Markus C. Knauer, Jurgen Kaminski, and Gerd Hausler, "Phase measuring deflectometry: a new approach to measure specular free-form surfaces," in *SPIE Optical Metrology in Production Engineering*, Wolfgang Osten and Mitsuo Takeda, Eds., Strasbourg, France, Sept. 2004, p. 366.

[6] Leopoldo Armesto, Josep Tornero, Alvaro Herraez, and Jose Asensio, "Inspection system based on artificial vision for paint defects detection on cars bodies," in *2011 IEEE International Conference on Robotics and Automation*, Shanghai, China, May 2011, pp. 1–4, IEEE.

[7] Pu Cheng, An Cui, Yujia Yang, Yawei Luo, and Wenlong Sun, "Recognition and classification of coating film defects on automobile body based on image processing," in *2017 10th International Congress on Image and Signal Processing, BioMedical Engineering and Informatics (CISP-BMEI)*, Shanghai, Oct. 2017, pp. 1–5, IEEE.

[8] Dimitris Manolakis, David Marden, and Gary A Shaw, "Hyperspectral Image Processing for Automatic Target Detection Applications," *Lincoln Laboratory Journal*, vol. 14, no. 1, pp. 38, 2003.

[9] J.C. Harsanyi and C.-I. Chang, "Hyperspectral image classification and dimensionality reduction: an orthogonal subspace projection approach," *IEEE Transactions on Geoscience and Remote Sensing*, vol. 32, no. 4, pp. 779–785, July 1994.

[10] Charles E. Miller, "Near-Infrared Spectroscopy of Synthetic Polymers," *Applied Spectroscopy Reviews*, vol. 26, no. 4, pp. 277–339, Dec. 1991.

[11] Frank A. DeThomas, Jeffrey W. Hall, and Stephen L. Monfre, "Real-time monitoring of polyurethane production using near-infrared spectroscopy," *Talanta*, vol. 41, no. 3, pp. 425–431, Mar. 1994.

[12] Xiaoyun Chen, Kshitish A. Patankar, and Matthew Larive, "Monitoring Polyurethane Foaming Reactions Using Near-Infrared Hyperspectral Imaging," *Applied Spectroscopy*, p. 0003702820941877, June 2020.

[13] Dimitris Manolakis, Eric Truslow, Michael Pieper, Thomas Cooley, and Michael Brueggeman, "Detection Algorithms in Hyperspectral Imaging Systems: An Overview of Practical Algorithms," *IEEE Signal Processing Magazine*, vol. 31, no. 1, pp. 24–33, Jan. 2014.

[14] Djordije Boskovic, Milica Orlandic, Sivert Bakken, and Tor Arne Johansen, "HW/SW Implementation of Hyperspectral Target Detection Algorithm," in *2019 8th Mediterranean Conference on Embedded Computing (MECO)*, Budva, Montenegro, June 2019, pp. 1–6, IEEE.

[15] William H. Farrand and Joseph C. Harsanyi, "Mapping the distribution of mine tailings in the Coeur d'Alene River Valley, Idaho, through the use of a constrained energy minimization technique," *Remote Sensing of Environment*, vol. 59, no. 1, pp. 64–76, Jan. 1997.